The unusual Kuiper belt object 2003 SQ317

Lacerda, P., McNeill, A., & Peixinho, N. (2014). The unusual Kuiper belt object 2003 SQ317. *Monthly Notices of the Royal Astronomical Society*, *437*(4), 3824-3831. https://doi.org/10.1093/mnras/stt2180

Published in:
Monthly Notices of the Royal Astronomical Society

Document Version:
Publisher's PDF, also known as Version of record

Monthly Notices of the ROYAL ASTRONOMICAL SOCIETY

MNRAS **437,** 3824–3831 (2014) doi:10.1093/mnras/stt2180
Advance Access publication 2013 December 3

The unusual Kuiper belt object 2003 SQ_{317}

Pedro Lacerda,[1★†] Andrew McNeill[1] and Nuno Peixinho[2,3]

[1] *Astrophysics Research Centre, School of Mathematics and Physics, Queen's University Belfast, Belfast BT7 1NN, UK*
[2] *Center for Geophysics of the University of Coimbra, Geophysical and Astronomical Observatory of the U. C., Almas de Freire, P-3040-004 Coimbra, Portugal*
[3] *Unidad de Astronomía, Universidad de Antofagasta, Avenida Angamos 601, Antofagasta, Chile*

Accepted 2013 November 7. Received 2013 November 3; in original form 2013 September 6

ABSTRACT

We report photometric observations of Kuiper belt object 2003 SQ_{317} obtained between 2011 August 21 and November 1 at the 3.58 m New Technology Telescope, La Silla. We obtained a rotational light curve for 2003 SQ_{317} with a large peak-to-peak photometric range, $\Delta m = 0.85 \pm 0.05$ mag, and a periodicity, $P = 7.210 \pm 0.001$ h. We also measure a nearly neutral broad-band colour $B - R = 1.05 \pm 0.18$ mag and a phase function with slope $\beta = 0.95 \pm 0.41$ mag deg^{-1}. The large light-curve range implies an extremely elongated shape for 2003 SQ_{317}, possibly as a single elongated object but most simply explained as a compact binary. If modelled as a compact binary near hydrostatic equilibrium, the bulk density of 2003 SQ_{317} is near 2670 kg m^{-3}. If 2003 SQ_{317} is instead a single, elongated object, then its equilibrium density is about 860 kg m^{-3}. These density estimates become uncertain at the 30 per cent level if we relax the hydrostatic assumption and account for solid, 'rubble pile'-type configurations. 2003 SQ_{317} has been associated with the Haumea family based on its orbital parameters and near-infrared colour; we discuss our findings in this context. If confirmed as a close binary, 2003 SQ_{317} will be the second object of its kind identified in the Kuiper belt.

Key words: techniques: photometric – Kuiper belt: general – Kuiper belt objects: individual: 2003 SQ_{317}.

1 INTRODUCTION

Haumea is a large, triaxial Kuiper belt object (KBO, semi-axes 2000 × 1600 × 1000 km), with a very fast rotation (period $P \approx 3.9$ h), a rock-rich interior (bulk density $\rho \approx 2500$ kg m^{-3}) and a surface covered in high-albedo ($p \approx 0.8$), nearly pure water ice, which shows signs of variegation (Rabinowitz et al. 2006; Lacerda & Jewitt 2007; Trujillo et al. 2007; Lacerda, Jewitt & Peixinho 2008; Lacerda 2009; Lellouch et al. 2010). Haumea has two, nearly coplanar satellites with similarly icy surfaces (Brown et al. 2005; Barkume, Brown & Schaller 2006; Dumas et al. 2011).

At least 10 other KBOs have been associated with Haumea on the basis that they have similar orbital elements and water-ice-rich surfaces (Brown et al. 2007; Ragozzine & Brown 2007; Schaller & Brown 2008; Snodgrass et al. 2010; Carry et al. 2012). The origin of this so-called Haumea family is unclear. Proposed ad hoc scenarios include a giant impact on to the proto-Haumea (Brown et al. 2007), a gentler graze-and-merge collision (Leinhardt, Marcus & Stewart 2010) and a sequence of two collisions in which the first creates a moon which is the target of the second collision (Schlichting & Sari 2009). The first scenario is ruled out by the low-velocity dispersion of the family members, while the last two possibilities are arguably improbable. Furthermore, the mass in the currently known family members and their velocity dispersion is not ideally matched by any of the proposed scenarios (Volk & Malhotra 2012).

Snodgrass et al. (2010) noticed that one member of the Haumea family, 2003 SQ_{317}, displayed large photometric variation, ~1 mag peak-to-peak, in just 14 measurements. They estimated a periodicity of about 3.7 h (or twice that) for this object. Such large variability in 200 km-scale objects often indicates extreme shapes from which useful information can be extracted (Hartmann & Cruikshank 1978; Weidenschilling 1980; Sheppard & Jewitt 2004; Lacerda & Jewitt 2007).

Here we report time-resolved, follow-up observations of 2003 SQ_{317} (hereafter SQ_{317}) obtained to clarify the nature of this object and the cause for the extreme variability and to improve our understanding of the Haumea family. We find that SQ_{317} indeed has an extreme shape, most simply explained by a compact binary, although more data are needed to rule out a single, elongated shape.

2 OBSERVATIONS

We observed KBO SQ_{317} using the 3.58 m ESO New Technology Telescope (NTT) located at the La Silla Observatory, in Chile. The NTT was configured with the EFOSC2 instrument (Buzzoni et al. 1984; Snodgrass et al. 2008) mounted at the *f*/11 Nasmyth focus and

★ E-mail: lacerda.pedro@gmail.com
† The presented data were obtained at the ESO facilities at La Silla under programmes 087.C-0980A and 088.C-0634A.

Table 1. Journal of observations. Columns are (1) UT date of observations, (2) heliocentric distance to KBO, (3) geocentric distance to KBO, (4) solar phase angle, (5) atmospheric seeing, (6) filters used, (7) exposure times used, and (8) atmospheric conditions.

Date UT	R (au)	Δ (au)	α (°)	Seeing (arcsec)	Filter	Exposure (s)	Conditions
2011 Aug 21	39.2440	38.4556	0.941	1.0	R	600	Photometric
2011 Aug 22	39.2440	38.4452	0.921	0.9	R	420	Photometric
2011 Aug 23	39.2440	38.4351	0.901	1.7	R,B	420, 600	Photometric
2011 Oct 30	39.2433	38.3911	0.748	0.8	R	300	Photometric
2011 Oct 31	39.2432	38.4003	0.769	0.7	R	300	Photometric
2011 Nov 01	39.2432	38.4097	0.790	0.8	R	300	Thin cirrus

Table 2. Photometry. Columns are (1) UT date of observations, (2) apparent R magnitude, (3) apparent B magnitude, (4) $B-R$ colour, and (5) absolute R magnitude, uncorrected for illumination phase darkening. All magnitudes are at maximum light-curve flux.

Date UT	m_R (mag)	m_B (mag)	$B-R$ (mag)	$m_R(1, 1, \alpha)$ (mag)
2011 Aug 21	22.44 ± 0.10	–	–	6.55 ± 0.10
2011 Aug 22	22.25 ± 0.03	–	–	6.36 ± 0.03
2011 Aug 23	22.29 ± 0.04	23.34 ± 0.18	1.05 ± 0.18	6.40 ± 0.04
2011 Oct 31	22.13 ± 0.04	–	–	6.24 ± 0.04
2011 Nov 01	22.23 ± 0.15	–	–	6.34 ± 0.15

equipped with a LORAL 2048 × 2048 CCD. We used the 2 × 2 binning mode bringing the effective pixel scale to 0.24 arcsec pixel^{-1}. Our observations were taken through Bessel B and R filters (ESO #639 and #642).

Each night, we collected bias calibration frames and dithered, evening and morning twilight flats through both filters. Bias and flat-field frames were grouped by observing night and then median-combined into nightly bias, and B and R flat-fields. The science images were also grouped by night and by filter and reduced (bias subtraction and division by flat-field) using the IRAF `ccdproc` routine. The R-band images suffered from slight fringing which was removed using an IRAF package optimized for EFOSC2 (Snodgrass & Carry 2013).

On photometric nights, we used observations of standard stars (MARK A1-3, 92 410, 94 401, PG2331+055B) from Landolt (1992) to achieve absolute calibration of field stars near SQ$_{317}$. We employed differential photometry relative to the calibrated field stars to measure the magnitude of SQ$_{317}$ as a function of time. Uncertainty in the differential photometry of SQ$_{317}$ (typically ±0.05 mag) was estimated from the dispersion in the measurements relative to different stars.

Table 1 presents a journal of the observations and Table 2 lists the calibrated, apparent magnitudes at peak brightness, measured for SQ$_{317}$ on photometric nights. Table 3 summarizes properties of SQ$_{317}$, both previously known and measured in this work.

3 RESULTS

3.1 Rotational light curve

Our photometry of SQ$_{317}$ resulted in $N = 154$ measurements over six nights spanning a total interval of $T = 1728$ h (Fig. 1), The brightness of SQ$_{317}$ varies visibly, by $\Delta m = 0.85 \pm 0.05$ mag peak-to-peak, taking only 1.8 h to go from minimum to maximum brightness. The full extent of this variation is seen on multiple nights.

To search for periodicity in the data we employed two methods: the phase dispersion minimization (PDM; Stellingwerf 1978) and the string-length minimization (SLM; Dworetsky 1983). PDM minimizes the ratio, Θ, between the scatter of the data phased with a trial period and that of the unphased data. The best-fitting period will result in a light curve with the least scatter, hence minimizing Θ. SLM minimizes the length of a segmented line connecting the data points phased with a trial period. Similarly to PDM, the best-fitting period will result in a light curve with the smallest scatter around the real, periodic light curve and hence the shortest string length. Before running the period-search algorithms we corrected the observing times by subtracting the light-travel time from SQ$_{317}$ to Earth for each measurement.

Fig. 2 shows the PDM periodogram for light-curve periods ranging from 3 to 11 h. Periods outside this range resulted in larger values of Θ. Two strong PDM minima are apparent, one at $P_{1/2} \approx 3.6$ h implying a single-peaked light curve with one maximum and one minimum per full rotation, and another at $P = 2 \times P_{1/2} \approx 7.2$ h which folds the data on to a double-peaked light curve (Fig. 1).

We favour the double-peaked solution, $P \approx 7.2$ h, for three reasons. First, a single-peaked light curve with a variation ∼0.85 mag would have to be caused by a peculiar, large contrast, surface albedo pattern. The symmetry and regularity of the light curve suggest that the brightness variation is modulated instead by the elongated shape of SQ$_{317}$ as it rotates; light curves produced by shape are double peaked. Secondly, the double-peaked solution produces a light curve with slightly asymmetric minima, seen on more than one night. The single-peaked light curve minimum exhibits more scatter suggesting that it is a superposition of two different minima. Finally, the single-peaked period, $P_{1/2} \approx 3.6$ h, would imply very fast rotation, at which SQ$_{317}$ would likely experience significant centripetal deformation for a plausible range of bulk densities and inner structures. The resulting elongated shape would produce a double-peaked light curve invalidating the premise that the light curve is single-peaked.

High-resolution analysis near the 7.2 h light curve indicates a PDM minimum at $P_{\rm PDM} = 7.210\,22$ h, while using the SLM method,

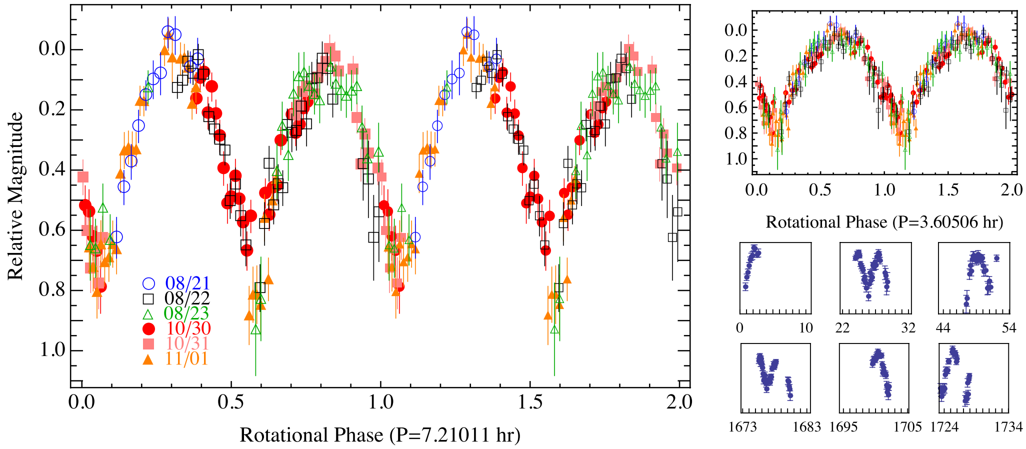

Figure 1. Light curve of SQ_{317}. Large panel shows data phased with the best-fitting spin period $P = 7.210\,11$ h. Two full rotations are shown. Smaller panels on the right show: (top) light curve phased with the possible but less likely period of $\sim$3.6 h, and (bottom) measurements on each individual night with the x-axis (time) labelled in hours since MJD 557 94.0 and the y-axis (unlabelled) equal to that of the figures above and to the left. The times are light-travel-time subtracted and so indicate when the light left SQ_{317}.

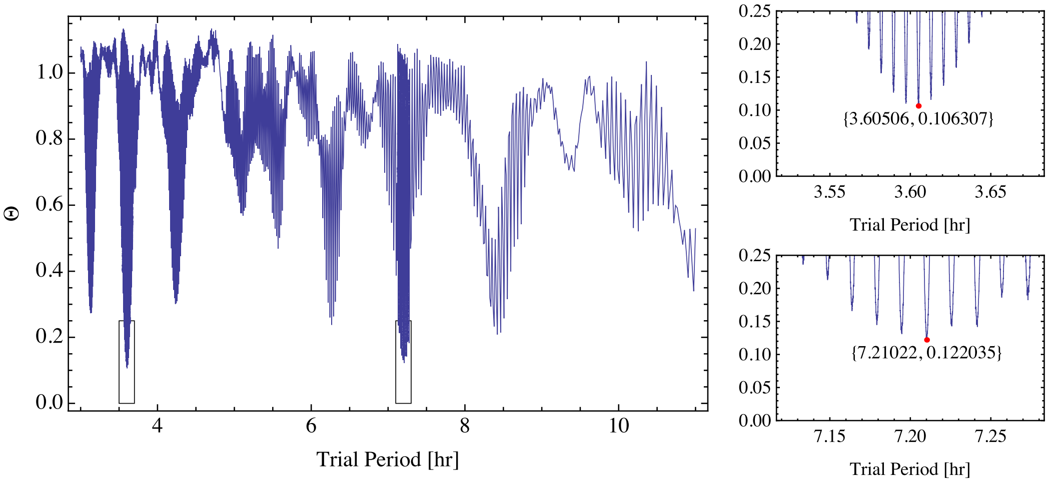

Figure 2. PDM periodogram for the SQ_{317} data. Minima of the quantity Θ mark the most likely rotational periods. The two deepest minima are marked with boxes and enlarged on the right; the best-fitting periods are shown in the insets together with the respective Θ value. Aliasing resulting from the way the data were sampled is visible in the insets.

we obtained a best-fitting period $P_{\mathrm{SLM}} = 7.209\,99$ h. We take as best-fitting solution the mean of the two, $P = 7.210\,11$ h. To estimate the uncertainty in our period solution, we employ (Horne & Baliunas 1986)

$$\delta f = \frac{3\pi\,\sigma_N}{2\sqrt{N}\,T\,\Delta m},$$

where δf is the uncertainty in the light-curve frequency, σ_N is the standard deviation of the light-curve best-fitting residuals (calculated using the model shown in Fig. 7), $N = 154$ is the number of data points, $T = 1728$ h is the total time spanned by the observations and $\Delta m = 0.85$ mag is the light-curve variation. The frequency uncertainty is $\delta f = 0.000\,02$ h^{-1} which corresponds to an uncertainty in the spin period $\delta P = 0.001\,03$ h. We therefore adopt as best period $P = 7.210 \pm 0.001$ h.

3.2 Phase curve

Owing to their large heliocentric distances, KBOs are only observable from Earth at small phase angles, $\alpha < 1\overset{\circ}{.}5$. Our observations span an approximate range $0.75 < \alpha\,[^\circ] < 0.95$, and we see a trend of fainter apparent magnitude with increasing phase angle. We fitted this observed phase darkening with a weighted linear model of the form

$$m_R(1, 1, \alpha) = m_R(1, 1, 0) + \beta\,\alpha,$$

where $m_R(1, 1, 0)$ is the absolute magnitude at zero phase angle and β is the linear phase curve coefficient. The fit is plotted in Fig. 3, where we show apparent magnitudes at light-curve maxima. The best-fitting zero-point and slope are $m_R(1, 1, 0) = 5.52 \pm 0.36$ mag and $\beta = 0.95 \pm 0.41$ mag deg^{-1}. If we disregard the two points with larger uncertainty (at $\alpha \approx 0\overset{\circ}{.}8$ and $\alpha \approx 0\overset{\circ}{.}95$), we obtain a comparable but more uncertain $m_R(1, 1, 0) = 5.57 \pm 0.60$ mag and $\beta = 0.88 \pm 0.68$ mag deg^{-1}. The phase function slope is steeper (although only by 2σ) than what is typically seen in other KBOs ($\beta_{\mathrm{KBO}} \sim 0.16$ mag deg^{-1}; Sheppard & Jewitt 2002; Rabinowitz, Schaefer & Tourtellotte 2007) and does not follow the trend for shallower phase functions observed in other objects associated with Haumea (Rabinowitz et al. 2008). We note that the phase function found above is consistent with the measurement $m_R = 22.05 \pm 0.02$ mag on 2008-08-30 (at phase angle

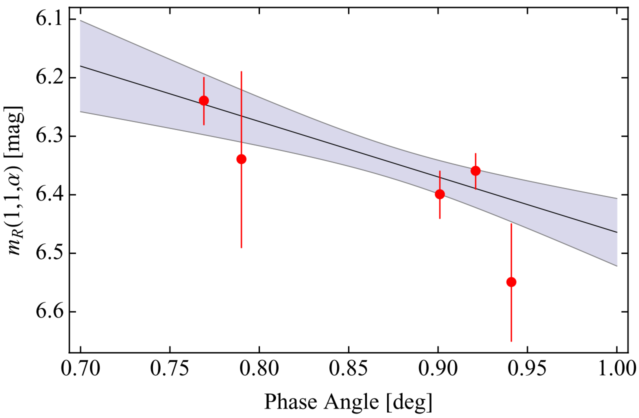

Figure 3. Phase curve of SQ$_{317}$ as inferred from five measurements (filled circles with error bars). A least-squares fit to the data is indicated as a black line within a shaded, 1σ confidence region. The best fit has a slope $\beta = 0.95 \pm 0.41$ mag deg^{-1} and intercept $m_R(1, 1, 0) = 5.52 \pm 0.36$ mag.

$\alpha = 0\overset{\circ}{.}62$, heliocentric distance $r = 39.261$ au and geocentric distance $\Delta = 38.342$ au) by Snodgrass et al. (2010). However, because of the narrow range of phase angles sampled, the uncertainty in the phase function slope is large so we are reluctant to draw strong implications from this result.

3.3 Shape model

The large photometric variability of SQ$_{317}$ suggests that the object has a highly elongated, possibly binary shape. Indeed, assuming that SQ$_{317}$ is close to hydrostatic equilibrium, its photometric range ($\Delta m = 0.85$ mag) and spin frequency ($\omega = 3.33$ d^{-1}) place it near the threshold between the Jacobi ellipsoid and the Roche binary sequences (Leone et al. 1984; Sheppard & Jewitt 2004). To explore this issue further, we attempt to fit the light curve of SQ$_{317}$ using Jacobi ellipsoid and Roche binary hydrostatic equilibrium models. The choice of models of hydrostatic equilibrium is physically based and has the benefit of allowing the density of SQ$_{317}$ to be estimated.

We follow the procedure detailed in Lacerda & Jewitt (2007) which considers a grid of models spanning a range of Jacobi ellipsoid shapes, and Roche binary shapes, mass ratios and separations calculated using the formalism in Chandrasekhar (1963). Each model is rendered at multiple rotational phases to extract the light curve. Surface scattering is modelled as a linear combination of the Lambert and Lommel–Seeliger laws. The former mimics a perfectly diffuse surface and adequately describes a high-albedo, icy object displaying significant limb darkening. The latter is meant to simulate a low-albedo, lunar-type surface with negligible limb darkening. These laws are linearly combined through a parameter, k, that varies between 0 (pure Lommel–Seeliger, lunar-type scattering) and 1 (pure Lambertian, icy-type scattering). The result is a collection of model light curves that can be compared to the one in Fig. 1 to identify the best-fitting model.

As described in Lacerda & Jewitt (2007), the Jacobi ellipsoid model light curves are fully defined by the model's triaxial shape (semi-axes A, B, C) in terms of the axis ratios B/A and C/A, and by the coefficient k. The Roche binary light curves are entirely described by the binary component mass ratio q, the primary triaxial shape defined by the axes ratios B/A and C/A, the secondary shape equally defined by the triaxial axis ratios b/a and c/a, the binary separation, $d \geq 1$ (expressed in units of the sum of the primary and secondary semi-axes $A + a$), and the scattering parameter, k.
Roche binaries are assumed to be tidally locked with the components aligned along their longest axes.

For simplicity and to keep the problem tractable, we consider only models viewed equator-on. Allowing the observing geometry to vary as a free parameter adds an extra dimension to our grid of models and, depending on how many aspect angles we consider, could take several weeks to compute. More importantly, this would only increase the degeneracy of the fitting procedure as we have light-curve data at a too restricted range of viewing angles to be able to constrain the spin pole orientation. Generally, off-equator geometries lead to slightly larger mass ratio solutions, but this has been shown not to have a significant effect on the inferred bulk density (Lacerda & Jewitt 2007), arguably the most important derived property.

Each model light curve is adjusted (in phase and offset) to the data using a Levenberg–Marquardt algorithm and the best-fitting one is selected using a χ^2 criterion. To explore the dependence of this procedure on the measurement uncertainties we employ a Monte Carlo approach: we generate $N = 371$ bootstrapped instances of the light curve of SQ$_{317}$ by randomizing each data point within its uncertainty error bar (errors are assumed normal with standard deviation equal to the size of the error bar). Finally, we find the best (minimum χ^2) model for each bootstrapped version light curve and thus obtain the distribution of best-fitting parameters.

Fig. 4 shows the best-fitting Jacobi ellipsoid light curve and Fig. 5 shows the corresponding model shape. The Monte Carlo

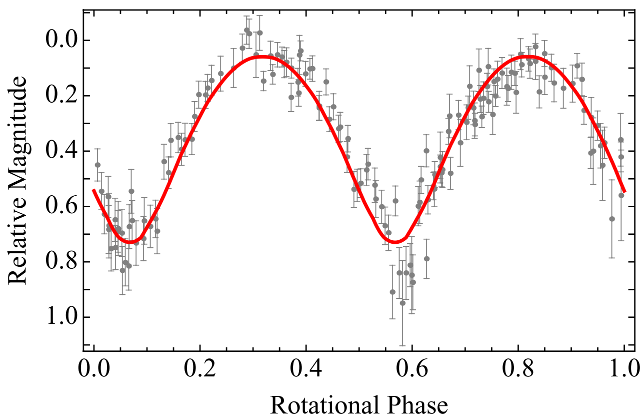

Figure 4. Best-fitting Jacobi ellipsoid light curve (solid line) plotted over the light-curve data for SQ$_{317}$ (grey points). The corresponding Jacobi ellipsoid is shown in Fig. 5.

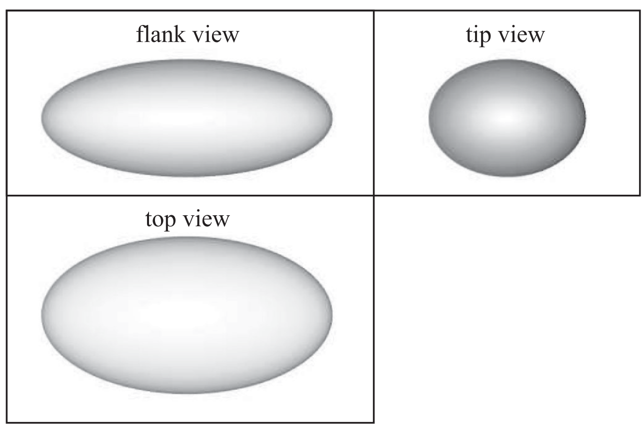

Figure 5. Jacobi ellipsoid model that best fits the light curve of SQ$_{317}$.

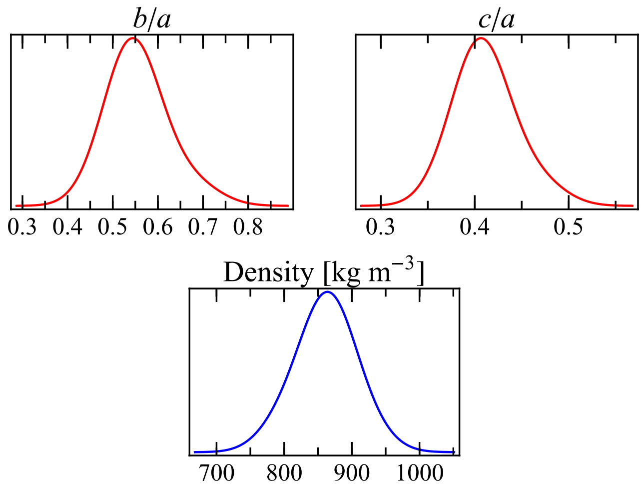

Figure 6. Monte Carlo distribution of Jacobi ellipsoid parameters (b/a and c/a) that fit the light curve of SQ_{317}. The Monte Carlo distribution of bulk density for these models is also shown.

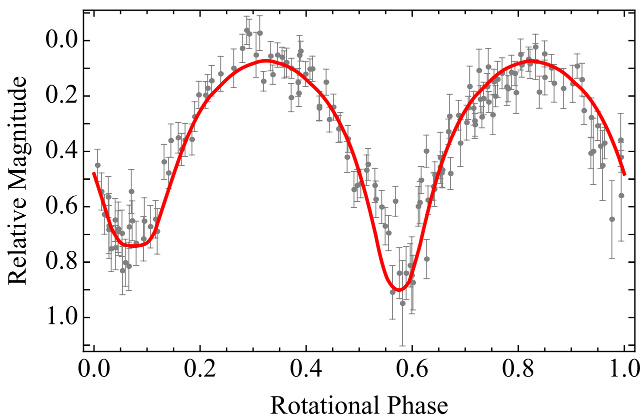

Figure 7. Best-fitting Roche binary light curve (solid line) plotted over the light-curve data for SQ_{317} (grey points). The corresponding Roche binary is shown in Fig. 8.

distributions of best-fitting parameters are shown in Fig. 6. Figs 7–9 show the best-fitting light curve, best model shape and parameter distributions for Roche binary models. Table 4 summarizes the best-fitting parameters for each model. The Roche binary fits are generally better with a typical $\chi^2 \approx 1.62$ per degree of freedom compared to $\chi^2 \approx 1.74$ per degree of freedom for the Jacobi ellipsoid models. The Roche binary model successfully fits the different minima in the light curve of SQ_{317}, unlike the Jacobi ellipsoid model. The mean scattering parameter for Jacobi ellipsoid fits is $k = 0.1$, consistent with a low-albedo surface, while for Roche binaries we find a mean $k = 0.4$, lending almost equal weights to (dark) lunar- and (bright) icy-type terrains. Higher k values imply stronger limb darkening, which is needed to fit the different light-curve minima.

3.4 Bulk density

In Section 3.3, we found the Jacobi ellipsoid and Roche binary that best fit the light curve of SQ_{317}. Because these models assume hydrostatic equilibrium, their shapes are uniquely related to bulk density and spin period and allow us to use the latter to constrain the former. Each model shape is a function of the dimensionless parameter $\Omega^2 = \omega^2/(\pi G\rho)$, where $\omega = 2\pi/P$ is the angular rotation frequency (P is the period), G is the gravitational constant and ρ is the bulk density. For a spin period $P = 7.21$ h, the density is then calculated as $\rho = 280/\Omega^2$ kg m^{-3}.

Predictably, the two types of model imply very different bulk densities (Figs 6 and 9, Table 4). The Jacobi model fit yields $\Omega^2 = 0.325 \pm 0.012$ and indicates a bulk density $\rho = 860 \pm 30\,\mathrm{kg\,m^{-3}}$, consistent with an icy composition. The Roche binary model has $\Omega^2 = 0.105 \pm 0.004$ and leads to $\rho = 2700 \pm 100\,\mathrm{kg\,m^{-3}}$, suggesting a rock-rich bulk composition for SQ_{317}.

4 DISCUSSION

As the analysis in Section 3.1 shows, SQ_{317} oscillates in brightness by $\Delta m = 0.85 \pm 0.05$ mag, making it the second most variable KBO known, only surpassed by 2001 QG_{298} (hereafter QG_{298}) with $\Delta m = 1.14 \pm 0.04$ mag (Sheppard & Jewitt 2004). For bodies in hydrostatic equilibrium, light-curve variation $\Delta m > 0.9$ mag can only plausibly be explained by a tidally distorted, binary shape (Weidenschilling 1980; Leone et al. 1984). That is the case of QG_{298} which was successfully modelled as a Roche binary leading to an estimated bulk density near $660\,\mathrm{kg\,m^{-3}}$ (Takahashi et al. 2004; Lacerda & Jewitt 2007; Gnat & Sari 2010). The Roche binary model received further support as QG_{298} was re-observed in 2010 to show a predicted decrease in variability to $\Delta m = 0.7$ magnitudes, which allowed the obliquity of the system to be estimated at very near 90° (Lacerda 2011).

With $\Delta m = 0.85$ mag and $P = 7.21$ h, SQ_{317} lies at the threshold between the Jacobi and Roche sequences (Leone et al. 1984; Sheppard & Jewitt 2004). Indeed, we find that SQ_{317} can be fitted reasonably well both by Jacobi and Roche models. However, one important feature of the light curve, the asymmetric light-curve minima, is only naturally fitted by the Roche binary model. The Jacobi model misses the data points that mark the faintest point of the light curve (Fig. 4). In theory, a special arrangement of brighter and darker surface patches could be adopted to ensure that the Jacobi model fit the fainter light-curve minimum. However, the binary model does not require any further assumptions and thus provides a simpler explanation for the asymmetric light-curve minima. Fig. 10 plots the change in light-curve variation, Δm, for both models. To maximize the change, we assumed the models to have 90° obliquity so that an angular displacement, ν, along the heliocentric orbit will translate into a change in aspect angle $\theta \approx \nu$ (Lacerda 2011). The two models produce slightly different behaviour and future observations may help rule out one of the solutions.

The Jacobi and Roche model solutions predict significantly different bulk densities for SQ_{317}. The former is consistent with a density around $860\,\mathrm{kg\,m^{-3}}$ which would indicate a predominantly icy interior and significant porosity. The Roche binary model implies a density close to $2670\,\mathrm{kg\,m^{-3}}$, consistent with a rocky bulk composition. Densities higher than $2000\,\mathrm{kg\,m^{-3}}$ have only been measured for the larger KBOs, Eris (Brown & Schaller 2007; Sicardy et al. 2011), Pluto (Null, Owen & Synnott 1993; Buie et al. 2006), Haumea (Rabinowitz et al. 2006; Lacerda & Jewitt 2007) and Quaoar (Fornasier et al. 2013). Densities for objects with diameters similar to SQ_{317} tend to fall in the range $500 < \rho < 1000\,\mathrm{kg\,m^{-3}}$ (Grundy et al. 2012; Stansberry et al. 2012) with the possible exception of (88611) Teharonhiawako with $\rho \approx 1400\,\mathrm{kg\,m^{-3}}$ (Osip, Kern & Elliot 2003; Lellouch et al. 2013). If confirmed, the Roche model density of SQ_{317} would make it one of the highest density known KBOs and the densest of its size.

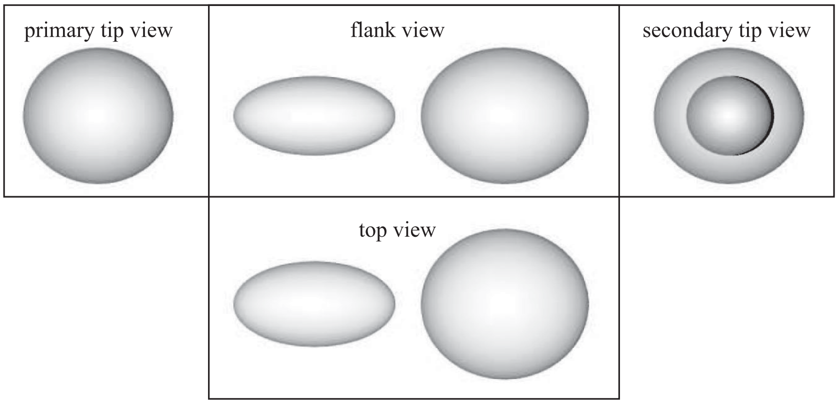

Figure 8. Roche binary model that best fits the light curve of SQ$_{317}$.

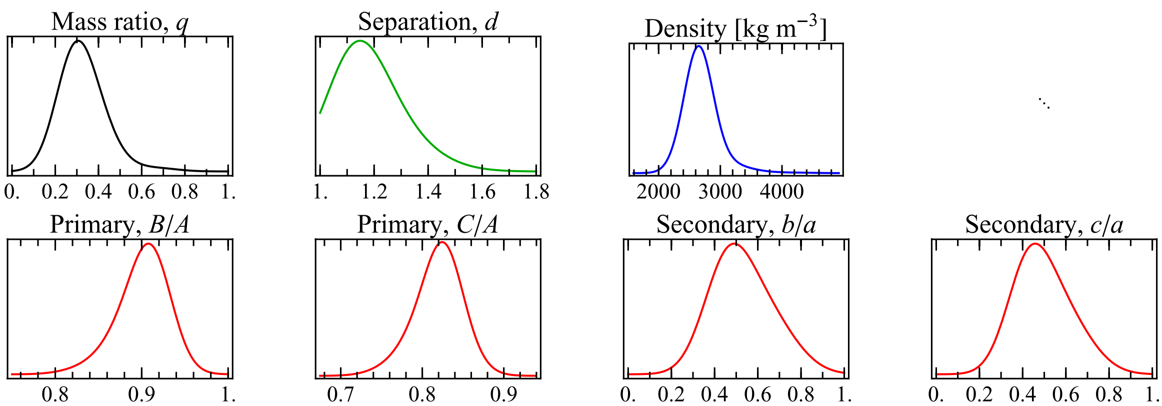

Figure 9. Monte Carlo distribution of Roche binary parameters (mass ratio q, binary separation d, B/A, C/A, b/a and c/a) that fit the light curve of SQ$_{317}$. The Monte Carlo distribution of bulk density for these models is also shown.

Table 3. Properties of SQ$_{317}$.

Orbital semimajor axis, a	42.753 au
Orbital eccentricity, e	0.082
Orbital inclination, i	28°.6
Equiv. diameter ($p = 0.50$), D	150 km
Equiv. diameter ($p = 0.05$), D	470 km
Absolute magnitude, $m_R(1, 1, 0)$	5.52 ± 0.36 mag
Phase function slope, β	0.95 ± 0.41 mag deg^{-1}
Light-curve period, P	7.210 ± 0.001 h
Light-curve variation, Δm	0.85 ± 0.05 mag

Note. Equivalent diameter is calculated from the measured absolute magnitude for two possible values of the geometric albedo using $D = (1329\,\mathrm{km})\, p^{-0.5}\, 10^{-0.2\, m_R(1,1,0)}$.

In a scenario in which the Haumea family was produced by a collision that ejected the volatile-rich mantle of the proto-Haumea, its members would be expected to be mainly icy in composition, with high-albedo surfaces. The Jacobi model density for SQ$_{317}$ would favour such a scenario (although the implied surface scattering is inconsistent with an icy, high-albedo and high limb-darkening surface) whereas the Roche model density would be harder to explain in the context of the family. Haumea's density $\rho \approx 2600\,\mathrm{kg\,m^{-3}}$ and water-ice spectrum implies a rocky core surrounded by a veneer of ice. If SQ$_{317}$ has high density and was produced from a collision on to Haumea, then it must be a fragment from the core material.

Broad-band near-infrared photometry of SQ$_{317}$ suggests a surface rich in water ice (Snodgrass et al. 2010). Our measurements indicate a nearly solar[1] surface colour $B - R = 1.05 \pm 0.18$ mag and a steep (although poorly constrained) phase function with slope $\beta = 0.95 \pm 0.41$ mag deg^{-1}. While the visible and infrared colours of SQ$_{317}$ match those of other members of the Haumea family, the phase function is much steeper.

The albedo of SQ$_{317}$ is unknown. Although its surface is blue and possibly water-ice rich, these properties do not necessary imply high albedo. For instance, 2002 MS$_4$ has blue colour ($B - R \approx 1.0$ mag; Peixinho et al. 2012) but low albedo ($p_V \approx 0.05$; Lellouch et al. 2013), and Quaoar displays strong water-ice absorption (Jewitt & Luu 2004) despite its relatively dark ($p_V \approx 0.12$; Lellouch et al. 2013) and red surface ($B - R \approx 1.6$ mag; Peixinho et al. 2012). Water ice has been spectroscopically detected on objects with albedos as low as 0.04, e.g. Chariklo (Guilbert et al. 2009), and as high as 0.80, e.g. Haumea (Trujillo et al. 2007).

The shape models and density estimates presented above assume an idealized fluid object in hydrostatic equilibrium. As a limiting case, the simplification is useful because it offers a simple and unique relation between shape, spin period and bulk density. However, SQ$_{317}$ is a solid body and likely behaves differently. Holsapple (2001, 2004) have studied extensively the equilibrium configurations of rotating solid bodies – sometimes termed 'rubble piles' – that possess no tensile strength but that can retain shapes bracketing the hydrostatic solution due to pressure-induced, internal friction. Similar studies were performed for Roche figures of equilibrium

[1] $(B - R)_{\odot} = 1.00 \pm 0.02$ mag (Holmberg, Flynn & Portinari 2006).

Table 4. Model fit parameters. Columns are (1) Model used to fit light curve, (2) component mass ratio, (3) binary separation in units of $A + a$, (4) and (5) primary semimajor axes, (6) and (7) secondary semimajor axes, and (8) model bulk density.

Model Type	q	d	B/A	C/A	b/a	c/a	ρ (kg m^{-3})
Jacobi ellipsoid	–	–	$0.55^{+0.05}_{-0.04}$	$0.41^{+0.02}_{-0.02}$	–	–	861^{+33}_{-32}
Roche binary	$0.32^{+0.08}_{-0.07}$	$1.14^{+0.14}_{-0.04}$	$0.91^{+0.01}_{-0.03}$	$0.82^{+0.01}_{-0.02}$	$0.51^{+0.15}_{-0.07}$	$0.48^{+0.13}_{-0.07}$	2671^{+88}_{-102}

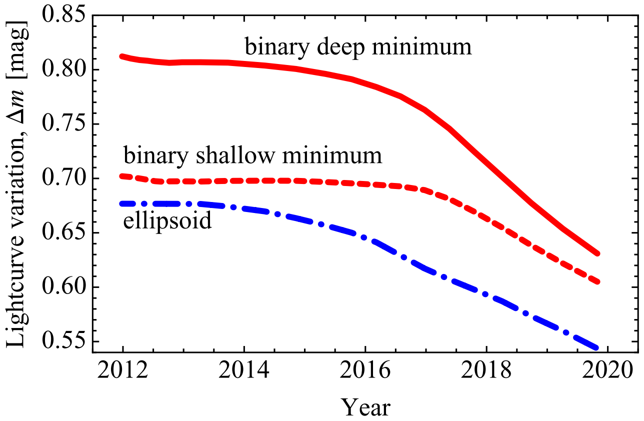

Figure 10. Model light-curve variation, Δm, as a function of time for the Jacobi ellipsoid (dash–dotted, blue) and the Roche binary solution. In the case of the binary model, the changes for the shallow (dashed, red) and deep (solid, red) minima are shown. The change in Δm plotted here is maximal as it assumes that the models have 90° obliquity initially.

by Sharma (2009). The deviation from the hydrostatic equilibrium solution is usually quantified in terms of an increasing angle of friction, $0° < \phi < 90°$. For a positive value of ϕ, a range of bulk densities (which includes the hydrostatic equilibrium solution) is possible for an object with a given shape and spin rate.

For a plausible range of albedos, SQ_{317} has an equivalent diameter in the range $150 < D < 450$ km. The giant planet icy moons in the same size range (Amalthea at Jupiter and Mimas, Phoebe and Janus at Saturn; Hyperion has chaotic rotation and is ignored) lie at the threshold between near hydrostatic shapes and slightly more irregular configurations (Thomas 2010; Castillo-Rogez et al. 2012). When approximated by triaxial ellipsoids and plotted on the diagrams of Holsapple (2001), the shapes, spins and densities of these moons are consistent with angles of friction $\phi < 5°$ (see also Sharma 2009). Similar values of ϕ are found for most large, approximately triaxial asteroids (Sharma, Jenkins & Burns 2009). If we take our Jacobi ellipsoid solution for SQ_{317} and assume an angle of friction $\phi = 5°$, then we find that its density should lie in the range $670 < \rho < 1100$ kg m^{-3}, i.e. a 30 per cent departure from the idealized hydrostatic equilibrium solution. A similar uncertainty applied to the Roche binary density estimate yields a range $2050 < \rho < 3470$ kg m^{-3}.

5 SUMMARY

We present time-resolved photometric observations of KBO SQ_{317} obtained in 2011 August and October to investigate its nature. Our results can be summarized as follows:

(i) SQ_{317} exhibited a highly variable photometric light curve with a peak-to-peak range $\Delta m = 0.85 \pm 0.05$ mag and period $P = 7.210 \pm 0.001$ h. The object has an almost solar broad-band colour $B - R = 1.05 \pm 0.18$ mag, making it one of the bluest KBOs known. The phase function of SQ_{317} is well matched by a linear relation with intercept $m_R(1, 1, 0) = 5.52 \pm 0.36$ mag and slope $\beta = 0.96 \pm 0.41$ mag deg^{-1}. This linear phase function is consistent with an earlier measurement obtained in 2008 at phase angle $\alpha = 0\overset{\circ}{.}62$.

(ii) The light curve implies that SQ_{317} is highly elongated in shape. Assuming that the object is in hydrostatic equilibrium, we find that the light curve of SQ_{317} is best fit by a compact Roche binary model with mass ratio $q \sim 0.3$, and triaxial primary and secondary components with axes ratios $B/A \sim 0.9$, $C/A \sim 0.8$ and $b/a \sim c/a \sim 0.5$, separated by $d \sim 1.1(A + a)$. The data are also adequately fitted by a highly elongated, Jacobi triaxial ellipsoid model with axes ratios $B/A \sim 0.55$ and $C/A \sim 0.41$. Observations in this decade may be able to rule out one of the two solutions.

(iii) If SQ_{317} is a Roche binary then its bulk density is approximately 2670 kg m^{-3}. This model-dependent density implies rock-rich composition for this object. However, if SQ_{317} is a Jacobi ellipsoid we find a significantly lower density, $\rho \approx 860$ kg m^{-3} consistent with an icy, porous interior. These density estimates become uncertain at the 30 per cent level if we relax the hydrostatic assumption and account for 'rubble pile'-type configurations.

ACKNOWLEDGEMENTS

We thank David Jewitt for comments, and Colin Snodgrass for supplying an IRAF fringe removal routine optimized for EFOSC2. PL acknowledges support from a Royal Society Newton Fellowship and from the Michael West Research Fellowship.

REFERENCES

Barkume K. M., Brown M. E., Schaller E. L., 2006, ApJ, 640, L87
Brown M. E., Schaller E. L., 2007, Science, 316, 1585
Brown M. E. et al., 2005, ApJ, 632, L45
Brown M. E., Barkume K. M., Ragozzine D., Schaller E. L., 2007, Nature, 446, 294
Buie M. W., Grundy W. M., Young E. F., Young L. A., Stern S. A., 2006, AJ, 132, 290
Buzzoni B. et al., 1984, The Messenger, 38, 9
Carry B., Snodgrass C., Lacerda P., Hainaut O., Dumas C., 2012, A&A, 544, A137
Castillo-Rogez J. C., Johnson T. V., Thomas P. C., Choukroun M., Matson D. L., Lunine J. I., 2012, Icarus, 219, 86
Chandrasekhar S., 1963, ApJ, 138, 1182
Dumas C., Carry B., Hestroffer D., Merlin F., 2011, A&A, 528, A105
Dworetsky M. M., 1983, MNRAS, 203, 917
Fornasier S. et al., 2013, A&A, 555, A15
Gnat O., Sari R., 2010, ApJ, 719, 1602
Grundy W. M. et al., 2012, Icarus, 220, 74
Guilbert A. et al., 2009, A&A, 501, 777
Hartmann W. K., Cruikshank D. P., 1978, Icarus, 36, 353
Holmberg J., Flynn C., Portinari L., 2006, MNRAS, 367, 449
Holsapple K. A., 2001, Icarus, 154, 432
Holsapple K. A., 2004, Icarus, 172, 272

Horne J. H., Baliunas S. L., 1986, ApJ, 302, 757
Jewitt D. C., Luu J., 2004, Nature, 432, 731
Lacerda P., 2009, AJ, 137, 3404
Lacerda P., 2011, AJ, 142, 90
Lacerda P., Jewitt D. C., 2007, AJ, 133, 1393
Lacerda P., Jewitt D., Peixinho N., 2008, AJ, 135, 1749
Landolt A. U., 1992, AJ, 104, 340
Leinhardt Z. M., Marcus R. A., Stewart S. T., 2010, ApJ, 714, 1789
Lellouch E. et al., 2010, A&A, 518, L147
Lellouch E. et al., 2013, A&A, 557, A60
Leone G., Paolicchi P., Farinella P., Zappala V., 1984, A&A, 140, 265
Null G. W., Owen W. M., Synnott S. P., 1993, AJ, 105, 2319
Osip D. J., Kern S. D., Elliot J. L., 2003, Earth Moon Planets, 92, 409
Peixinho N., Delsanti A., Guilbert-Lepoutre A., Gafeira R., Lacerda P., 2012, A&A, 546, A86
Rabinowitz D. L., Barkume K., Brown M. E., Roe H., Schwartz M., Tourtellotte S., Trujillo C., 2006, ApJ, 639, 1238
Rabinowitz D. L., Schaefer B. E., Tourtellotte S. W., 2007, AJ, 133, 26
Rabinowitz D. L., Schaefer B. E., Schaefer M., Tourtellotte S. W., 2008, AJ, 136, 1502
Ragozzine D., Brown M. E., 2007, AJ, 134, 2160
Schaller E. L., Brown M. E., 2008, ApJ, 684, L107
Schlichting H. E., Sari R., 2009, ApJ, 700, 1242
Sharma I., 2009, Icarus, 200, 636
Sharma I., Jenkins J. T., Burns J. A., 2009, Icarus, 200, 304
Sheppard S. S., Jewitt D. C., 2002, AJ, 124, 1757
Sheppard S. S., Jewitt D., 2004, AJ, 127, 3023
Sicardy B. et al., 2011, Nature, 478, 493
Snodgrass C., Carry B., 2013, The Messenger, 152, 14
Snodgrass C., Saviane I., Monaco L., Sinclaire P., 2008, The Messenger, 132, 18
Snodgrass C., Carry B., Dumas C., Hainaut O., 2010, A&A, 511, A72
Stansberry J. A. et al., 2012, Icarus, 219, 676
Stellingwerf R. F., 1978, ApJ, 224, 953
Takahashi S., Shinokawa K., Yoshida F., Mukai T., Ip W. H., Kawabata K., 2004, Earth, Planets Space, 56, 997
Thomas P. C., 2010, Icarus, 208, 395
Trujillo C. A., Brown M. E., Barkume K. M., Schaller E. L., Rabinowitz D. L., 2007, ApJ, 655, 1172
Volk K., Malhotra R., 2012, Icarus, 221, 106
Weidenschilling S. J., 1980, Icarus, 44, 807

This paper has been typeset from a TEX/LATEX file prepared by the author.